https://doi.org/10.5194/egusphere-2022-610
Preprint. Discussion started: 28 July 2022

The response of ocean climate change to different heat-flux perturbations over North Atlantic in FAFMIP

Wenyu Yin[1,2], Xin Gao[1], Jiangbo Jin[1,3*], Yi Yu[3], Guangqing Zhou[1*], Qingcun Zeng[1]

[1]*International Center for Climate and Environment Sciences, Institute of Atmospheric Physics, Chinese Academy of Sciences, Beijing* 100029, *China*

[2]*College of Earth and Planetary Sciences, University of Chinese Academy of Sciences, Beijing* 100049, *China*

[3]*State Key Laboratory of Satellite Ocean Environment Dynamics, Second Institute of Oceanography, Ministry of Natural Resources, Hangzhou 310012, China*

* Corresponding author: Jiangbo Jin and Guangqing Zhou

Email: jinjiangbo@mail.iap.ac.cn and zhgq@mail.iap.ac.cn

https://doi.org/10.5194/egusphere-2022-610
Preprint. Discussion started: 28 July 2022

Abstract

The diversity of surface flux perturbations, especially for heat-flux perturbations, notably results in uncertainties surrounding the responses of ocean climate change under the global warming scenarios projected by climate/earth system models. However, when imposing heat-flux perturbations on the models, there are strong feedbacks between atmosphere and ocean, causing nearly doubled heat-flux perturbation over North Atlantic (NA). In this study, we quantitatively evaluated the impacts of magnitude changes of heat-flux perturbations over NA on the changes in the Atlantic Meridional Overturning Circulation (AMOC), ocean heat uptake (OHU) and dynamic sea level (DSL) by analyzing eight model responses to the heat flux perturbations experiments in Flux-Anomaly-Forced Model Inter-comparison Project (FAFMIP). We found that the magnitude of the AMOC change was very sensitive to the magnitude change of imposed NA heat-flux perturbation, and the weakening amplitude of the AMOC was nearly halved as the imposed heat-flux perturbation F halved over the NA. The most significant responses of both DSL and OHU to the magnitude changes of NA heat-flux perturbation were mainly found in the Atlantic and Arctic (AA) basin, especially for the NA region. Both the added ocean heat uptake (OHUa) and redistributed ocean heat uptake (OHUr) play roles in OHU changes among the different NA heat-flux perturbation experiments. The magnitude change of NA-mean OHUa was almost linearly related to the imposed NA heat-flux perturbation, while the magnitude change of NA-mean OHUr, which is mainly caused

https://doi.org/10.5194/egusphere-2022-610
Preprint. Discussion started: 28 July 2022

by AMOC change and redistributed heat flux, was not proportional to the imposed NA heat-flux perturbation.

Key Words: heat-flux perturbation; ocean heat uptake; North Atlantic; Atlantic Meridional Overturning Circulation; coupled general circulation model

https://doi.org/10.5194/egusphere-2022-610
Preprint. Discussion started: 28 July 2022

1 Introduction

The ocean climate change under the global warming scenario is of great significance for human survival and development. The ocean climate change includes changes in the Atlantic Meridional Overturning Circulation (AMOC), the dynamic sea level (DSL) and the ocean heat uptake (OHU). The changes in AMOC are mainly induced by buoyancy forcing, including heat-flux and freshwater flux perturbation (Bouttes et al, 2014), in the North Atlantic (NA), and the AMOC changes are also tightly coupled to the redistribution of OHU (Banks and Gregory, 2006; Huber and Zanna, 2017). The thermal expansion of seawater due to OHU is a major contributor to the rise in the global-mean sea level, accounting for 21-43% of the total rise projected for the years 2081-2100 under a mid-range-emission scenario (SSP2/RCP4.5) (Hermans et al, 2021). Coupled climate/earth system models are widely used to predict climate change of DSL, AMOC and OHU under global warming, but there are large uncertainties in the results (Yin et al, 2010; Yin, 2012; Eyring et al, 2016; Weijer et al, 2020; Jin et al, 2021). Thus, it is vitally important to investigate the uncertainties surrounding ocean climate change under global warming scenarios.

The 1% yr^{-1} CO_2 increase (1pctCO_2) experiment initialized in a preindustrial control state is a baseline experiment for all the phases of the Coupled Model Inter-comparison Project (CMIP), which refers to a series of climate change experiments exploring how the climate system responds to greenhouse gas forcing.

https://doi.org/10.5194/egusphere-2022-610
Preprint. Discussion started: 28 July 2022

However, the DSL change shows different patterns in 1pctCO_2 experiments among different climate models (Church et al, 2013; Pardaens et al, 2011). The spreads across models may come from the differences of initial fields (i.e. different preindustrial control states), the differences of the surface-flux perturbation (including the heat flux, freshwater flux, and momentum flux) or the differences of coupled model formulation.

Bouttes and Gregory (2014) pointed out that differences in preindustrial control (piControl) states have little impact on the diversity of sea-level changes. Furthermore, many previous studies showed that the differences in surface-flux perturbations, especially for heat-flux perturbations, could be major factors causing the differences in model-estimated ocean climate change under global warming (Stammer et al,2011; Slangen et al,2014; Jin et al, 2021). The momentum-flux and heat-flux perturbations play important roles in reproducing the key features of sea-level change, such as the dipole patterns over the NA (positive to the north of 40°N, negative to the south), the Southern Ocean (positive to the north of 50°S, negative to the south) and the North Pacific (positive to the south of 40°N, negative to the north) (Xie et al, 2012; Bouttes et al, 2012; Bouttes et al, 2014). Most of the AMOC weakening and OHU are caused by surface heat-flux perturbations (Huber and Zanna, 2017). Notably, the diverse patterns of CO_2-forced sea-level changes cannot be totally reproduced by imposing several sets of surface-flux perturbation (simulated by different coupled models) on a single model (Bouttes et al, 2014). Bouttes et al. (2014) proposed that part of the

https://doi.org/10.5194/egusphere-2022-610
Preprint. Discussion started: 28 July 2022

diversity in sea-level changes, which cannot be explained by different surface-flux perturbation forcing, may be related to the differences in ocean model formulation of coupled models.

To determine the roles that different model formulations play in contributing to the inter-model uncertainty regarding ocean climate change under global warming, the CMIP6 launched the Flux-Anomaly-Forced Model Inter-comparison Project (FAFMIP) to compare the responses of different models to consistent surface-flux perturbations (Gregory et al, 2016). The surface-flux perturbations in the FAFMIP are derived from the ensemble-mean differences between years 61 and 80 of the 13 CMIP5 atmosphere–ocean coupled models of a 1pctCO_2 scenario experiment (corresponding to a doubled CO_2 concentration). By applying a same set of surface flux perturbations to different CMIP6 models, the FAFMIP excludes the diversity that arises directly from surface-flux perturbations simulated by different Atmospheric-Oceanic General Circulation Models (AOGCMs).

Consistent with the previous work, the heat-flux perturbation, especially the heat-flux perturbation over NA, is the most dominant factor leading to ocean climate change among all the surface flux perturbations in FAFMIP (Rahmstorf and Ganapolski, 1999; Gregory et al, 2016; Jin et al, 2021). However, when imposing heat-flux perturbations on the models, the prescribed heat flux perturbations induce the changes in ocean circulation, which redistribute the ocean heat and the sea surface temperature (SST),

https://doi.org/10.5194/egusphere-2022-610
Preprint. Discussion started: 28 July 2022

causing strong redistributed feedback on heat flux over NA (Gregory et al, 2016). A quantitative evaluation of the influence of different magnitudes of heat-flux perturbations over the NA on the ocean climate change under global warming has been lacking. In this study, we mainly focused on the heat-flux perturbation experiments (faf-heat, faf-heat-NA50pct, faf-heat-NA0pct and faf-passiveheat) in the FAFMIP to quantitatively evaluate the impacts of the magnitude changes of heat-flux perturbations in the NA region on the changes in the AMOC, OHU and DSL.

The paper is structured as follows: the details of the models and methods are introduced in Section 2, the results are detailed in Section 3, and the discussion and summary are presented in Section 4.

2 The experiments, method and models:

2.1 Experiments

The FAFMIP is designed to isolate the ocean uncertainty by imposing a fixed set of surface flux (the heat flux, freshwater flux, and momentum flux) perturbation, which are obtained as the ensemble-mean difference of the monthly-mean flux in the CMIP5 1pctCO_2 simulation at double CO_2 concentration relative to the corresponding monthly mean flux in the control simulation. The FAFMIP includes seven experiments: one equivalent to a piControl experiment with an extra passive tracer

https://doi.org/10.5194/egusphere-2022-610
Preprint. Discussion started: 28 July 2022

(faf-passiveheat), three experiments with individual applications of flux perturbations (faf-heat, faf-water and faf-stress), and one experiment with all the perturbations (faf-all). Additionally, two new experiments, faf-heat-NA50pct and faf-heat-NA0pct experiments, are attached to FAFMIP. Although method B (as described below) was applied in the heat-flux perturbation experiments, the heat flux imposed to the models was not applied as intended. Since the prescribed heat flux perturbations induce the changes in ocean density, which lead to changes in advection and diffusion, causing a change in ocean heat transport and SST. The SST changes, in turn, result in strong redistributed feedback on heat flux. The redistributed heat-flux Q_r' has significant influence over the NA region, nearly doubles the prescribed heat flux perturbation F over NA. The newly added experiments are designed to figure out the influence of unintended exaggerated heat flux over NA on ocean climate changes. This study evaluated the output from three heat-flux perturbation experiments and faf-passiveheat in the FAFMIP, as described below:

The faf-heat experiment: a perturbation of the heat flux was directly imposed on the ocean surface temperature as an external heat-flux forcing. Large positive heat-flux perturbation was occurs in the mid–high-latitude NA region (about 80°W–10°E, 30–65°N) and in the Southern Ocean (78°S-35°N). To eliminate the strong negative feedback between the surface heat flux and SST and to maximize the effect of the prescribed surface heat-flux perturbation, we adopted the tracer approach method B recommended by the FAFMIP.

https://doi.org/10.5194/egusphere-2022-610
Preprint. Discussion started: 28 July 2022

The faf-heat-NA50pct experiment: the experiment was exactly the same as the faf-heat experiment except that the heat-flux perturbation in the NA was multiplied by 50% within a portion of the NA region, as proposed at the FAFMIP meeting in April 2019. The purpose of this experiment was to reproduce the simulation which is similar to that in 1pctCO_2 experiments, since the faf-heat experiment provided greater weakening because of the redistribution feedback (Gregory et al, 2016; Couldrey et al, 2020).

The faf-heat-NA0pct experiment: This experiment was similar to faf-heat and faf-heat-NA50pct but with a zero perturbation in the NA region, as was also proposed at the FAFMIP meeting in April 2019.

The faf-passiveheat experiment: The experiment was equivalent to the piControl experiment. The heat-flux perturbation was applied to surface without affecting the evolution of the ocean state. The passive tracer T_a initialized to zero, which can be used to diagnose the effect of added heat on ocean temperatures due to ocean circulation changes through a comparison of faf-passiveheat with other heat-flux perturbation experiments.

2.2 Methods

For the three heat-flux perturbation experiments in the FAFMIP, the method used by

Bouttes et al. (2014) as "method B" in the FAFMIP is recommended for computing the heat flux. According to Gregory et al. (2016), when the heat flux perturbation is applied to the surface layer, surface air temperature rise, significantly reducing the net surface heat flux into ocean. The strong negative feedback damps the effect of prescribed surface heat-flux perturbation, F. In order to maximize the effect of F on the sea surface, two tracers are introduced in method B: the added temperature tracer, T_a, and redistributed temperature tracer, T_r. T is the sum of T_a and T_r and refers to total ocean temperature change. T_r was used to calculate the SST and surface heat flux, T was applied to compute the seawater density. The main difference between T and T_r is that T_r was not directly forced by the prescribed heat-flux perturbation F. Thus, the SST cannot be directly affected by heat flux perturbation and the SST-heat flux negative feedback was damped. The redistributed tracer, T_r, and T were both initialized with the same piControl state, and transported by the same velocities and diffusion coefficients. The prescribed heat-flux perturbation F resulted in the temperature change,T, which lead to changes in ocean density, ocean circulation and oceanic heat transport, causing indirect influence on the SST change.

The added tracer, T_a, was only affected by the prescribed surface heat-flux perturbation, F, which was initialized at zero, and mainly reflected the influence of the prescribed heat-flux perturbation F. The T_a change ($T_a{}'$) was calculated from the difference in T_a between the heat-flux perturbation experiments and faf-passiveheat. The $T_a{}'$ equation for the heat-flux perturbation experiments can be schematically

https://doi.org/10.5194/egusphere-2022-610
Preprint. Discussion started: 28 July 2022

expressed as follows:

$$\frac{\partial T_a{}'}{\partial t} = -\nabla \cdot (v\, T_a{}') + F \tag{1}$$

where $\nabla \cdot (v\, T_a{}')$ is the transport operator and v includes all the transport and diffusion processes.

The T_r change ($T_r{}'$) was calculated from the difference in T_r between the heat-flux perturbation experiments and faf-passiveheat, which resulted from the ocean transport change (including changes in advection and diffusion) and redistributed heat-flux $Q_r^{'}$, the corresponding $T_r{}'$ can be expressed as follows:

$$\frac{\partial T_r^{'}}{\partial t} = -\nabla \cdot (v_c T_r{}' + v' T_c) + Q_r^{'} \tag{2}$$

where the first term to the right of Equation (2) is the ocean transport change due to the temperature change, $v_c T_r{}'$, and the circulation change, $v' T_c$. The subscript c denotes the state in the faf-passiveheat experiment (control experiment).

The temperature change (T') calculated from the difference between the heat-flux perturbation and faf-passiveheat can be regarded as the sum of $T_r{}'$ and $T_a{}'$.

$$T_r{}' + T_a{}' = T' \tag{3}$$

2.3 The calculation of sea-level change

The DSL change can be divided into the steric sea-level (SSL) change due to the

https://doi.org/10.5194/egusphere-2022-610
Preprint. Discussion started: 28 July 2022

density change in the seawater and the mass sea-level (MSL) change due to the convergence and divergence caused by the ocean circulation change; the MSL is calculated from the difference between the DSL and SSL. The SSL equation can be schematically expressed as follows:

$$SSL = -\int_{-H}^{0} \frac{\rho(T,S) - \rho(T_R,S_R)}{\rho(T_R,S_R)} dz \tag{4}$$

where ρ is the seawater density; T is the temperature of the seawater; S is the salinity of the seawater; T_R and S_R are the temperature and salinity averaged over years 61-70, respectively; and H is the depth of the ocean. Additionally, the SSL change can be divided into the halosteric sea level (HSSL) and thermosteric sea level (TSSL).

The TSSL and HSSL equations can be schematically expressed as follows:

$$TSSL = -\int_{-H}^{0} \frac{\rho(T,S_R) - \rho(T_R,S_R)}{\rho(T_R,S_R)} dz \tag{5}$$

$$HSSL = -\int_{-H}^{0} \frac{\rho(T_R,S) - \rho(T_R,S_R)}{\rho(T_R,S_R)} dz \tag{6}$$

2.4 Models

In this study, we analyzed the responses of eight CMIP6 AOGCMs (ACCESS, CAS-ESM2, CanESM5, FGOALS-g3, GFDL-ESM2M, MPI-ESM1-2-HR, MRI-ESM2.0 and MIROC6) involved in the FAFMIP heat flux perturbation experiments; the details of the eight models are presented in Table 1. The output from the faf-heat experiment are available for all the models except the AMOC in GFDL-

https://doi.org/10.5194/egusphere-2022-610
Preprint. Discussion started: 28 July 2022

ESM2M, but some of the output from the faf-heat-NA50pct and faf-heat-NA0pct experiments is not available. And not all the variables were submitted for some models. For instance, the AMOC of GFDL-ESM2M and DSL of MIROC6 are not available for faf-heat-NA50pct. And MPI-ESM1-2-HR did not conduct a faf-heat-NA0pct experiment. The AMOC of GFDL-ESM2M and MIROC6, and the DSL of MIROC6 are not available for faf-heat-NA0pct. The details of the available data are described in Table2.

The ensemble-mean in this paper were averaged across all the available output data of the eight models. Both the horizontal and vertical model fields were linearly interpolated to the same grid as CAS-ESM2 for the ensemble-mean. The ocean component of CAS-ESM2 is with a 1° zonal resolution between 78.5°S and 87.5°N ,and a meridional resolution refined to 0.5° between 10°S and 10°N, increased gradually from 0.5° to 1° between 10° and 20°. The AMOC change, DSL change, temperature change and OHU were defined as the differences of the three heat-flux perturbation experiments (faf-heat, faf-heat-NA50pct and faf-heat-NA0pct) simulation relative to faf-passiveheat experiment simulation of corresponding years.

3 Results

3.1 AMOC change

The imposed heat-flux perturbation enhances the ocean stratification by increasing the temperature *T* over NA, which might reduce the convection and weakens the AMOC.

Figure 1 shows the time series of the AMOC strength change relative to faf-passiveheat for the three heat-flux perturbation experiments. The strength of the AMOC is defined as the maximum of the overturning stream function between 20°N and 70°N in the Atlantic, and between the depths of 300 m and 2000 m, calculated from the residual overturning stream function (Yang et al, 2016). AMOC weakening was exhibited in all the models for the faf-heat and faf-heat-NA50pct experiments. All models showed continuous AMOC declines in the first decades and gradually reached a quasi-equilibrium state at around 50 years in faf-heat and faf-heat-NA50pct. For the faf-heat-NA0pct experiment, most of the models exhibited slight weakening of the AMOC; only CanESM5 and FGOALS-g3 showed a positive change in the AMOC strength.

The magnitude of the AMOC weakening is very sensitive to the magnitude change of heat-flux perturbation over the NA region. The AMOC changes for faf-heat, faf-heat-NA50pct and faf-heat-NA0pct averaged over the final decade were -11.33 ± 3.98, -6.88 ± 2.74 and -1.06 ± 1.57 Sv (ensemble-mean AMOC change ± standard deviation), respectively. This reveals that the AMOC weakening was nearly proportional to the NA heat-flux perturbation, F, and the slight AMOC weakening in faf-heat-NA0pct may result from the effect of the F outside the NA. The model spreads of AMOC changes averaged over the final decade range from -6.02 to -16.14 Sv in faf-heat and from -5.32 to -10.35 Sv in faf-heat-NA50pct. In the faf-heat-NA0pct experiment, the corresponding spread ranged from -2.44 to 1.07 Sv.

https://doi.org/10.5194/egusphere-2022-610
Preprint. Discussion started: 28 July 2022

The AMOC weakening would prevent warm seawater being transported northward from the low latitudes to high latitudes in the Atlantic, strengthening the T_r cooling over the high-latitude Atlantic and the T_r warming over the low-latitude Atlantic. Since the sea surface turbulence flux is calculated by T_r, the T_r cooling over the NA would lead to positive Q_r' into the ocean in the NA region, which in turn, enhances the AMOC weakening, resulting in positive feedback. However, SST cooling due to the AMOC weakening decreases the stratification and helps with convection activity, which damps AMOC weakening, resulting in negative feedback. The redistributed heat-flux Q_r' over NA is a result from the combination of these two feedbacks. Gregory et al. (2016) pointed out that the Q_r' is nearly equal to F over the NA in the faf-heat experiment. To further confirm whether the Q_r' was equal to F over the NA in the two newly added faf-heat-NA50pct and faf-heat-NA0pct experiments, Figure 2 shows the patterns of the ensemble-mean Q_r' averaged in the final decade. As expected, the Q_r' shows a positive pattern over the NA in both the faf-heat and faf-heat-NA50pct experiments, but the Q_r' shows a negative pattern over the NA in the faf-heat-NA0pct experiment. The full integration averages of the Q_r' over the NA are about 9.49W/m^2 and 0.12W/m^2 in faf-heat and faf-heat-NA0pct, respectively. In the faf-heat-NA50pct experiment, the 70-year-mean Q_r' (4.64W m^{-2}) is almost equal to the prescribed F (4.96W m^{-2}) over the NA, which verifies that the Q_r' doubles the prescribed F over the NA in faf-heat-NA50pct. The total heat flux, F+Q_r' (9.60W m^{-2}), in faf-heat-NA50pct is approximately equal to the prescribed F (9.92W m^{-2}) in

https://doi.org/10.5194/egusphere-2022-610
Preprint. Discussion started: 28 July 2022

faf-heat, suggesting that the prescribed F in faf-heat over the NA can be roughly reproduced by the total heat flux (F+$Q_r^{'}$) imposed in faf-heat-NA50pct. Additionally, there is a strong anti-correlation between the $Q_r^{'}$ in the NA region and AMOC change, and the coefficients are -0.80 and -0.57 in faf-heat and faf-heat-NA50pct, respectively.

Outside the NA regions, there are almost similar patterns in the $Q_r^{'}$ differences of faf-heat-NA0pct relative to faf-heat-NA50pct, and faf-heat-NA50pct relative to faf-heat (Figure 2d and 2e): a positive difference occurred in the Arctic, west coast of the Pacific and tropical and mid-latitude south Atlantic, and negative differences were found in the equatorial Pacific and mid-latitude Indian. This indicates that the imposed heat flux over the NA had a remote influence on these regions.

3.2 OHU

Figure 3 shows the time series of the volume-mean temperature changes (T', $T_r{}'$ and $T_a{}'$) in the three experiments. Although the rate of the temperature change differed, there were substantial increases in T' in all the experiments. The increase in T' was dominated by $T_a{}'$ (Figure 3a-f) for all the models in all three experiments. The most significant increase in the ensemble-mean T' was observed in faf-heat, followed by faf-heat-NA50pct, and the weakest increase was observed in faf-heat-NA0pct. For instance, the global-mean T' averaged at the final year were 0.23±0.05, 0.19±0.03 and 0.14±0.03°C (global-mean T' ensemble-mean±standard deviation) for the three

https://doi.org/10.5194/egusphere-2022-610
Preprint. Discussion started: 28 July 2022

perturbation experiments, respectively. This indicates that halving the heat perturbation over the NA would reduce the global-mean T' by about 0.05℃. The global-mean T_a' averaged at the final year accounts for 78-86% of the T', and the remaining part is attributed to Q_r'. There were large spreads in the global-mean T' exhibited among the models in all three experiments. For example, the model spreads in T' at the final year ranged from 0.17 to 0.30 ℃, 0.15 to 0.25 ℃, and 0.13 to 0.20 ℃ in faf-heat, faf-heat-NA50pct and faf-heat-NA0pct, respectively. The corresponding model spreads in T_a' ranged from 0.17 to 0.18 ℃, 0.14 to 0.16 ℃, and 0.11 to 0.13 ℃ in the three experiments, respectively. The model spreads in T_a' can only account for 10-20% of the spreads of T', suggesting that the model spreads of T' in the three experiments mainly result from T_r' rather than T_a'. The results from FGOALS-g3 showed outliers for T' (0.13 ℃ in faf-heat, 0.09 ℃ in faf-heat-NA50pct, and 0.03 ℃ in faf-heat-NA0pct), which might be due to the larger negative changes in the sea ice cover or SST of FGOALS-g3 than in other models (Wang et al, 2020).

To find out how different basins responded to different NA heat-flux perturbations, we divided the global ocean into the Pacific-Indo Ocean (PI, 22°–134°E and 35°S–65°N), the Arctic and Atlantic Ocean (AA, 35°S–90°N) and the Southern Ocean (SO, 78°S–35°N). The vertical profiles of the temperature change averaged over the final decade in the different basins are presented in Figure 4. The basin-scale T' and T_a' increases were confined to the upper ocean (upper 2 km) in the SO and PI basins, and the AA basin temperature change penetrated into deeper layers relative to the SO and

https://doi.org/10.5194/egusphere-2022-610
Preprint. Discussion started: 28 July 2022

PI basins. The ensemble-mean T' in the PI and SO basins was dominated by T_a'. Around 75% (faf-heat)-97% (faf-heat-NA0pct) of the ensemble-mean vertical-averaged T' was attributable to the T_a' in the SO basin. The vertical-averaged T' values were 0.26±0.04, 0.21±0.03 and 0.18±0.01 ℃ (T' ensemble-mean±standard deviation), and the T_a' values were 0.19±0.02, 0.18±0.01 and 0.18±0.01 ℃ (T_a' ensemble-mean±standard deviation) in the SO basin for faf-heat, faf-heat-NA50pct and faf-heat-NA0pct experiments, respectively. For the PI basin, the T_a' was equal to 84% (faf-heat)-102% (faf-heat-NA0pct) of the T' in the three heat-flux perturbation experiments. The vertical-averaged T' values were 0.17 ±0.02, 0.16±0.01 and 0.14±0.01 ℃ in the three experiments, respectively, while the T_a' values were about 0.14±0.01℃ for all the three experiments. Comparing the increasing T' and T_a' values, we can see the magnitude changes in T_a' among the three heat-flux experiments only accounted for 10% of the magnitude changes in T', which indicates the magnitude changes in T' mainly arose from the T_r' in the SO and PI basins. This also implies that the effects of T_r' in the PI and SO basins are different for the three experiments, with warming in the PI and SO basins in faf-heat and faf-heat-NA50pct, and weak cooling in the PI basin in faf-heat-NA0pct. The close similarities of the T' and T_a' in the PI and SO basins in the three heat-flux perturbation experiments reveal that the magnitude change of NA heat-flux perturbations have little influence on the T' and T_a' of the PI and SO basins.

The AA basin is the region that was most affected by the prescribed heat perturbation

https://doi.org/10.5194/egusphere-2022-610
Preprint. Discussion started: 28 July 2022

over the NA (Figure 4c and 4f). The magnitude changes among the three experiments are much larger than the changes in the SO and PI basins. The vertical-averaged T' values were 0.27±0.04, 0.18±0.03 and 0.10±0.02 °C, and the vertical-averaged T_a' were 0.33 ± 0.05, 0.21 ± 0.03 and 0.07 ± 0.03 °C in the AA basin in faf-heat, faf-heat-NA50pct and faf-heat-NA0pct, respectively. There were large inconsistences between the T' and T_a' in AA basin in all the three experiments, which implies that the T' in the AA basin was not only dominated by the T_a', but the T_r' also played a non-negligible role. The ensemble-mean T_a' in the AA basin was approximately 120% of the T' for faf-heat and faf-heat-NA50pct, which means that the basin-scale T_r' tended to make a negative contribution up to 20% of the T'. However, the T_r' in faf-heat-NA0pct made a positive contribution to the T', accounting for 30% of the T' in faf-heat-NA0pct. Additionally, there were substantial disagreements in the T' and T_a' across the models shown in the AA basin, which may be related to the different degrees of AMOC weakening across the models (Figure 3).

The OHU is one of the key indicators of global climate change, and it is determined by temperature change. Figure 5 shows the patterns of the OHU ($\int \rho c_p T' dz$), added ocean heat uptake ($\int \rho c_p T_a' dz$) (OHUa) and redistributed ocean heat uptake ($\int \rho c_p T_r' dz$) (OHUr) in the final decade. A significant positive OHU mainly occurred in the AA and SO basins in all the three experiments (Figure 5a-c). Consistent with the vertical profiles of the temperature changes, the OHU was dominated by OHUa in the SO and PI basins, while the OHU was charged by both the OHUa and OHUr in

https://doi.org/10.5194/egusphere-2022-610
Preprint. Discussion started: 28 July 2022

the AA basin in all three experiments (i.e. Figure 5b, 5e and 5h). The positive OHUa mainly appeared in the NA and SO region (Figure 5d-f). The positive OHUrs were observed in the south low-to-mid-latitude Atlantic and the Equatorial Pacific, while the negative OHUr could be observed in the NA and Arctic regions in all the three experiments (Figure 5g-i).

The most significant difference in the OHU among the three experiments was located in the AA basin, especially in the NA region (Figure 5a-c). The difference in OHUa caused by the NA heat-flux perturbations was located in the NA and Arctic (Figure 5d-f), and the difference in OHUr was located in the Atlantic for the three experiments (Figure 5g-i). As mentioned above, the ocean circulation change has huge influence on ocean heat transport, which affects the ocean heat redistribution. The difference in the OHU over the NA resulted from the combined effect of the OHUa and OHUr. For the NA region, the ensemble-mean regional-mean OHUs were 6.36, 3.00 and 0.68 GJ/m^2 in faf-heat, faf-heat-NA50pct and faf-heat-NA0pct, respectively. The corresponding NA-mean OHUas were 10.33, 6.70 and 1.31 GJ/m^2 in the three experiments, respectively, making a crucial contribution to the OHU in the NA region. The magnitude change in OHUa over the NA among the three experiments was roughly proportional to the imposed F over the NA, which indicates the influence of the circulation changes on the $T_a{}'$ was relatively small. The NA-mean OHUrs were -3.97, -3.70 and -0.63 GJ/m^2 in the three experiments, respectively. The magnitude change in OHUr over the NA among the three experiments was not proportional to the

https://doi.org/10.5194/egusphere-2022-610
Preprint. Discussion started: 28 July 2022

imposed NA heat-flux perturbation, which may be related to the ocean heat transport.

For the regions out of the NA, the ensemble-mean regional-mean OHUr warming at low latitudes (30°N-30°S) of the Atlantic were 3.76, 1.94 and 0.82 GJ/m^2 in the three experiments, respectively. The low-latitude Atlantic warming due to the OHUr was closely related to the AMOC weakening. The correlation coefficient between the low-latitude regional-mean OHUr and AMOC change is -0.87 in faf-heat and -0.96 in faf-heat-NA50pct for the available models. This is consistent with previous studies showing that most of the warming at low latitudes results from tropical heat convergence and reduced northward heat transport due to a weakened AMOC (Gregory et al, 2016; Dias et al, 2020b; Couldrey et al, 2021). In addition, the SO regional-mean OHU would increase by 0.25 GJ/m^2 as half of the prescribed heat flux ,F, over the NA was added to the ocean, which implies that the magnitude change of the heat flux perturbation over NA has a remote influence on the SO, but the connections are unclear.

The largest model spreads in the OHU were mainly located in the AA basin, specifically, in the NA region (Figure 6). The standard deviations of the OHU over NA were 3.55, 2.86 and 1.46 GJ/m^2 in faf-heat, faf-heat-NA50pct and faf-heat-NA0pct, respectively. The standard deviation of the OHU accounts for more than 50% of the ensemble-mean change of OHU. The standard deviation of the OHUa accounts for less than 25% of the ensemble-mean change in faf-heat and

https://doi.org/10.5194/egusphere-2022-610
Preprint. Discussion started: 28 July 2022

faf-heat-NA50pct, which were only 2.45 GJ/m^2 in faf-heat and 1.70 GJ/m^2 in faf-heat-NA50pct. The standard deviation of OHUr over NA is almost equal to ensemble mean change, ranging from 3.66 GJ/m^2 in faf-heat to 1.05GJ/m^2 in faf-heat-NA0pct. This further demonstrates that the model spreads of the OHU over the NA are mainly attributable to the model spreads of the OHUr over the NA in all three heat-flux perturbation experiments.

3.3 DSL change

The patterns of the multi-model ensemble-mean changes in the DSL, HSSL and TSSL averaged over the final decade in the three experiments are shown in Figure 7. The common spatial characteristics of the DSL changes are shown in all the three experiments: the diploes in the Antarctic Circumpolar Current (ACC) region (positive in the north, switching to negative values further south) and the North Pacific (positive south of 40^{o}N to negative further north, Figure 7a-c), which mainly resulted from the TSSL change (Gregory et al, 2016; Todd et al, 2020; Couldrey et al, 2021).The TSSL changes pattern resemble to the OHU. The most obvious differences in the DSL change among the three experiments were observed in the NA, which was affected by both the TSSL change and HSSL change. The positive DSL change covered the whole regions of the NA in the faf-heat experiment, with a strong positive DSL change at the north of 40°N due to the combined effects of the positive TSSL and HSSL changes, and a weak positive DSL change at the south of 40°N resulted

https://doi.org/10.5194/egusphere-2022-610
Preprint. Discussion started: 28 July 2022

from the countervailing influence of the positive TSSL change and negative HSSL change (Figure 7d and 7g). Compared to faf-heat, a weaker positive DSL change over NA was observed in faf-heat-NA50pct, and even a negative DSL change appeared over 20-40°W in the NA, which mainly resulted from the smaller magnitude of the TSSL and HSSL changes, especially the negative TSSL change over the east of NA. Inconsistent with the simulations of the faf-heat and faf-heat-NA50pct experiments, the DSL change in faf-heat-NA0pct exhibited a significant negative pattern over most areas of the NA (Figure 7c), which mainly resulted from the weakened positive HSSL change and negative TSSL change in faf-heat-NA0pct (Figure 7f and 7i). The regional-mean DSL changes over NA are 0.17, 0.06 and 0.00m in faf-heat, faf-heat-NA50pct and faf-heat-NA0pct, respectively (Figure 7a-c). The TSSL components contribute 0.15, 0.03 and -0.03m (Figure 7d-f) and HSSL components contribute 0.02, 0.03 and 0.03m (Figure 7g-i) to the DSL change over NA in the three experiments, respectively.

The substantial model spreads of the DSL were mainly located in the NA region and Arctic (Figure 8a-c), which resulted from the combined effects of the spreads of the TSSL and HSSL. The standard deviation of the DSL change was almost of the same order as the ensemble-mean change in DSL in the three experiments. Interestingly, the standard deviations of the TSSL and HSSL changes were even larger than the ensemble-mean TSSL and HSSL changes in the three experiments. This suggests there are large uncertainties surrounding the TSSL and HSSL changes over the NA

https://doi.org/10.5194/egusphere-2022-610
Preprint. Discussion started: 28 July 2022

across the models. However, the model spreads of the DSL change, the combination of the spreads of TSSL and HSSL change, are much smaller. The standard deviations of the DSL over the NA were 0.13, 0.05 and 0.03m in faf-heat, faf-heat-NA50pct and faf-heat-NA0pct, respectively. The standard deviations of the TSSL over the NA were at around 0.18m, and the standard deviations of the HSSL were 0.12, 0.10 and 0.07m in the three experiments, respectively.

4 Summary and discussion

In this study, we quantitatively evaluated how climate/earth system models responded to the different magnitudes of heat-flux perturbations in the NA region by comparing the outputs of the three heat-flux perturbation experiments (faf-heat, faf-heat-NA50pct and faf-heat-NA0pct) and faf-passiveheat in the FAFMIP, focusing on the changes in the AMOC, OHU and DSL. We found that the magnitude of the AMOC weakening is sensitive to the imposed NA heat-flux perturbation, consistent with the results of Bouttes et al. (2014). It is notable that the AMOC weakening is nearly proportional to the imposed *F* over NA. The heat-flux perturbation outside the NA region has little effect on the AMOC weakening (only -1.06 Sv in faf-heat-NA0pct). Large model spreads of AMOC weakening are still observed, especially in the faf-heat experiment.

There is a significant anti-correlation between the Q_r' over the NA and AMOC change, the coefficient reached -0.80 in faf-heat. The SST cooling over the NA region due to AMOC weakening enhance the positive heat flux over NA, which further enhance the AMOC weakening ,while the SST cooling decreases the stratification simultaneously, which damps AMOC weakening .The two effects together lead to a positive $Q_r^{'}$ over NA. The total heat flux (F+$Q_r^{'}$) nearly doubles the intended heat-flux perturbation imposed on the NA region in faf-heat-NA50pct, which is consistent with the results of faf-heat experiment. Therefore, the effect of the intended F over the NA in faf-heat can be roughly reproduced by the total heat flux (F+$Q_r^{'}$) imposed over the NA in faf-heat-NA50pct.

The global mean T' mainly results from the $T_a{}'$ in all the three experiments, accounting for 78-86% of the T'. Halving the perturbation over the NA would reduce the global-mean T' by about 0.05 ℃ (accounting for 20% of the T'). Different basins respond differently to the magnitude change of heat-flux over NA. T' is dominated by $T_a{}'$ in the SO and PI basins, while most of the magnitude changes in T' among the three heat-flux perturbation experiments are attributable to $T_r{}'$ instead of $T_a{}'$ in the SO and PI basins. The AA basin is most affected by the prescribed heat perturbation over the NA. Different from the PI and SO basins, the T' is charged by both the $T_a{}'$ and $T_r{}'$ in the AA basin, and both the magnitude changes in $T_a{}'$ and $T_r{}'$ play roles in determining the magnitude changes in T' among the heat-flux perturbation experiments. There are substantial disagreements across the models for T' and $T_a{}'$ shown in the AA basin, which may be related to the different degrees of

https://doi.org/10.5194/egusphere-2022-610
Preprint. Discussion started: 28 July 2022

AMOC weakening across the models.

Consistent with basin-scale T', the most significant difference in the OHU among the three experiments was observed in the AA basin, especially in the NA region. The differences in both OHUa and OHUr in the three experiments have a strong influence on the total OHU difference over the NA region. This is consistent with the findings of previous work (Gregory et al, 2016; Dias et al, 2020b; Couldrey et al, 2021). The magnitude change in OHUa over the NA is almost proportional to the imposed heat flux over the NA. However, the magnitude change in OHUr over the NA is not proportional to the imposed NA heat-flux perturbation, which may be attributed to the heat transport due to the ocean circulation change. It is worth mentioning that we find the magnitude change of low-latitude OHUr in Atlantic is closely related to AMOC change, with a correlation coefficient up to -0.87. The largest model spreads of the OHU are located in the NA region. The standard deviation of OHU and OHUr over NA are almost of the same order as the ensemble-mean change of them, indicating that there are large disagreements across the models for the OHU and OHUr.

Magnitude change of heat-flux perturbations over the NA had little influence on the dipole patterns in the North Pacific and SO. The largest DSL change response to different NA heat-flux perturbations was observed in the NA, which is affected by both the TSSL change and HSSL change. As the heat flux perturbation over NA region decreases, the magnitude of the positive DSL change over the NA region tends

https://doi.org/10.5194/egusphere-2022-610
Preprint. Discussion started: 28 July 2022

to be weakened, and even turn to be significant negative pattern over most parts of NA. There are substantial model spreads of the DSL for the NA region, which result from the combined effects of the spreads of the TSSL and HSSL. The standard deviation of the DSL change is almost of the same order as the ensemble-mean change in the three experiments.

Reducing the perturbation in the NA would result in changes in the ocean interior processes, such as resolved advection, parameterized eddy advection, isopycnal mixing, and diapycnal mixing, which would benefit the further understanding of changes in OHU including global and basin scales. Evaluating the ocean interior processes will be our initial focus on future work. Another point is to figure out how the heat-flux perturbation changes over NA affect other basins and how the tele-connections are built.

https://doi.org/10.5194/egusphere-2022-610
Preprint. Discussion started: 28 July 2022

Acknowledgement. *This work was jointly supported by the National Natural Science Foundation of China (Grant No 41991282), the Strategic Priority Research Program of the Chinese Academy of Sciences (Grant No. XDB42000000), the National Natural Science Foundation of China (Grant Nos. 41630530) and the open fund of the State Key Laboratory of Satellite Ocean Environment Dynamics, Second Institute of Oceanography (Grant No. QNHX2017). The simulations in this study were sponsored by the National Key Scientific and Technological Infrastructure project "Earth System Science Numerical Simulator Facility" (EarthLab).*

https://doi.org/10.5194/egusphere-2022-610
Preprint. Discussion started: 28 July 2022

Reference

Banks, H. T. and Gregory, J. M.: Mechanisms of ocean heat uptake in a coupled climate model and the implications for tracer-based predictions of ocean heat uptake, Geophys. Res. Lett., 33, L07608, https://doi.org/10.1029/2005GL025352, 2006.

Bouttes, N., Gregory, J. M., Kuhlbrodt, T., and Suzuki, T.: The effect of wind stress change on future sea level change in the Southern Ocean, Geophys. Res. Lett., 39, L23602, https://doi.org/10.1029/2012GL054207, 2012.

Bouttes, N. and Gregory, J. M.: Attribution of the spatial pattern of CO_2-forced sea level change to ocean surface flux changes, Environ. Res. Lett., 9, 034004, https://doi.org/10.1088/1748-9326/9/3/034004, 2014.

Bouttes, N., Gregory, J. M., Kuhlbrodt, T., and Smith, R. S.: The drivers of projected North Atlantic sea level change, Clim. Dynam., 43, 1531–1544, https://doi.org/10.1007/s00382-013-1973-8, 2014.

Church, J. A., Clark, P. U., Cazenave, A., Gregory, J. M., Jevrejeva, S., Levermann, A., Merrifield, M. A., Milne, G. A., Nerem, R. S., Nunn, P. D., Payne, A. J., Pfeffer, W. T., Stammer, D., and Unnikrishnan, A. S.: Sea Level Change, in: Climate Change 2013: The Physical Science Basis. Contribution of Working Group I to the Fifth Assessment Report of the Intergovernmental Panel on Climate Change, edited by: Stocker, T. F., Qin, D., Plattner, G.-K., Tignor, M., Allen, S. K., Boschung, J., Nauels, A., Xia, Y., Bex, V., and Midgley, P. M.,

https://doi.org/10.5194/egusphere-2022-610
Preprint. Discussion started: 28 July 2022

Cambridge University Press, https://doi.org/10.1017/CBO9781107415324.026, 2013

Couldrey, M. P., Gregory, J. M., Boeira Dias, F., Dobrohotoff, P., Domingues, C. M., Garuba, O., Griffies S. M., Haak, H., Hu, A., Ishii, M., Jungclaus, J., Köhl, A., J.Marsland, S., Ojha, S., Saenko, O. A., Savita, A., Shao, A., Stammer, D., Suzuki, T., and Zanna, L.: What causes the spread of model projections of ocean dynamic sea-level change in response to greenhouse gas forcing?, Clim. Dynam., 56, 155-187, https://doi.org/10.1007/s00382-020-05471-4, 2021.

Dunne, J. P., John, J. G., Hallberg, R. W., Griffies, S. M., Shevli akova, E. N., Stouffer, R. J., Krasting, J. P., Sentman, L. A., Milly, P. C. D., Malyshev, S. L., Adcroft, A. J., Cooke, W., Dunne, K. A., Harrison, M. J., Levy, H., Samuels, B. L., Spelman, M., Winton, M., Wittenberg, A. T., Phillips, P. J., and Zadeh, N.: GFDL's ESM2 global coupled climate-carbon Earth System Models Part I: Physical formulation and baseline simulation characteristics, J. Climate, 25, 6646–6665, https://doi.org/10.1175/JCLI-D11-00560.1, 2012.

Dias, F. B., Fiedler, R., Marsland, S. J., Domingues, C. M., Clément, L., Rintoul, S. R., Mcdonagh, E. L., Mata, M. M. and Savita, A.: Ocean heat storage in response to changing ocean circulation processes, J. Climate, 33, 9065-9082, https://doi.org/10.1175/JCLI-D-19-1016.1, 2020.

Eyring, V., Bony, S., Meehl, G. A., Senior, C. A., Stevens, B., Stouffer, R. J., and Taylor, K. E.: Overview of the Coupled Model Intercomparison Project Phase 6

(CMIP6) experimental design and organization, Geosci. Model Dev., 9, 1937–1958, https://doi.org/10.5194/gmd-9-1937-2016, 2016.

Gregory, J. M., Bouttes, N., Griffies, S. M., Haak, H., Hurlin, W. J., Jungclaus, J., Kelley, M., Lee, W. G., Marshall, J., Romanou, A., Saenko, O. A., Stammer, D., and Winton, M.: The Flux-Anomaly-Forced Model Intercomparison Project (FAFMIP) contribution to CMIP6: investigation of sea-level and ocean climate change in response to CO_2 forcing, Geosci. Model Dev., 9, 3993–4017, https://doi.org/10.5194/gmd-9-3993-2016, 2016.

Hermans, T. H. J., Gregory, J. M., Palmer, M. D., Ringer, M. A., Katsman, C. A., and Slangen, A. B. A.: Projecting global mean sea‐level change using CMIP6 models, Geophys. Res. Lett., 48, e2020GL092064, https://doi.org/10.1029/2020GL092064, 2021.

Huber, M. B. and Zanna, L.: Drivers of uncertainty in simulated ocean circulation and heat uptake, Geophys. Res. Lett., 44, 1402– 1413, https://doi.org/10.1002/2016GL071587, 2017.

Jin, J. B., Zhang, H., Dong, X., Liu, H. L., Zhang, M. H., Gao, X., He, J. X., Chai, Z. Y., Zeng, Q.C., Zhou, G.Q., Lin, Z.H., Yu, Y., Lin, P.F., Lian, R., Yu, Y.Q., Song, M.R., and Zhang, D.L.: CAS-ESM2. 0 Model datasets for the CMIP6 flux-anomaly-forced model intercomparison project (FAFMIP), Adv. Atmos. Sci., 38, 296-306, https://doi.org/10.1007/s00376-020-0188-2, 2021.

Jin, J., Dong, X., He, J., Yu, Y., Liu, H., Zhang, M., Zeng, Q., Zhang, H., Gao, X., Zhou, G., and Wang, Y.: Ocean Response to a Climate Change Heat-Flux

https://doi.org/10.5194/egusphere-2022-610
Preprint. Discussion started: 28 July 2022

Perturbation in an Ocean Model and Its Corresponding Coupled Model, Adv. Atmos. Sci., 39,55-66, https://doi.org/10.1007/s00376-021-1167-y, 2022.

Kiss, A. E., Hogg, A. McC., Hannah, N., Boeira Dias, F., Brassington, G. B., Chamberlain, M. A., Chapman, C., Dobrohotoff, P., Domingues, C. M., Duran, E. R., England, M. H., Fiedler, R., Griffies, S. M., Heerdegen, A., Heil, P., Holmes, R. M., Klocker, A., Marsland, S. J., Morrison, A. K., Munroe, J., Nikurashin, M., Oke, P. R., Pilo, G. S., Richet, O., Savita, A., Spence, P., Stewart, K. D., Ward, M. L., Wu, F., and Zhang, X.: ACCESS-OM2 v1.0: a global ocean–sea ice model at three resolutions, Geosci. Model Dev., 13, 401–442, https://doi.org/10.5194/gmd-13-401-2020, 2020.

Li, L., Yu, Y., Tang, Y., Lin, P., Xie, J., Song, M., Dong, L., Zhou, T., Liu, L., Wang, L., Pu, Y., Chen, X., Chen, L., Xie, Z., Liu, H., Zhang, L., Huang, X., Feng, T., Zheng, W., Xia, K., Liu, H., Liu, J., Wang, Y., Wang, H., Jia, B., Xie, F., Wang, B., Zhao, S., Yu, Z., Zhao, B. and Wei, J.: The flexible global ocean-atmosphere-land system model grid-point version 3 (fgoals-g3): description and evaluation, J. Adv. Model. Earth Sy., 12, e2019MS002012, https://doi.org/10.1029/2019MS002012, 2020.

Mauritsen, T., Bader, J., Becker, T., Behrens, J., Bittner, M., Brokopf, R., Brovkin, V., Claussen, M., Crueger, T., Esch, M., Fast, I., Fiedler, S., Fläschner, D., Gayler, V., Giorgetta, M., Goll, D. S., Haak, H., Hagemann, S., Hedemann, C., Hohenegger, C., Ilyina, T., Jahns, T., Jimenéz-de-la-Cuesta, D., Jungclaus, J., Kleinen, T., Kloster, S., Kracher, D., Kinne, S., Kleberg, D.,

https://doi.org/10.5194/egusphere-2022-610
Preprint. Discussion started: 28 July 2022

Lasslop, G., Kornblueh, L.,Marotzke, J., Matei, D., Meraner, K., Mikolajewicz, U., Modali, K., Möbis, B., Müller, W.A., Nabel, J.E.M. S. Nam, C. C. W., Notz, D., Nyawira, S., Paulsen, H., Peters, K., Pincus, R., Pohlmann, H., Pongratz, J., Popp, M., Raddatz, T. J., Rast, S., Redler, R., Reick, C. H., Rohrschneider, T., Schemann, V., Schmidt, H., Schnur, R., Schulzweida, U., Six, K. D., Stein, L., Stemmler, I., Stevens, B.,Jin-Song von Storch, Tian, F., Voigt, A., Vrese, P., Wieners, K., Wilkenskjeld, S., Winkler, A., and Roeckner, E.: Developments in the MPI‐M Earth System Model version 1.2 (MPI-ESM1. 2) and its response to increasing CO_2, J. Adv. Model. Earth Sy., 11,998-1038, https://doi.org/10.1029/2018MS001400, 2019.

Pardaens, A. K., Gregory, J. M., and Lowe, J. A.: A model study of factors influencing projected changes in regional sea level over the 21st century, Clim. Dynam., 36, 2015–2033, doi:10.1007/s00382-009-0738-x, 2011.

Rahmstorf S, and Ganopolski, A.: Long-term global warming scenarios computed with an efficient coupled climate model, Clim. Change, 43, 353-367, https://doi.org/10.1023/A:1005474526406, 1999.

Slangen, A. B. A., Carson, M., Katsman, C. A., van de Wal, R. S. W., Köhl, A., Vermeersen, L. L. A., and Stammer, D.: Projecting twenty-first century regional sea-level changes, Clim. Change, 124, 317–332, https://doi.org/10.1007/s10584-014-1080-9, 2014.

https://doi.org/10.5194/egusphere-2022-610
Preprint. Discussion started: 28 July 2022

Stammer, D., Agarwal, N., Herrmann, P., Köhl, A., and Me choso, C. R.: Response of a Coupled Ocean-Atmosphere Model to Greenland Ice Melting, Surv. Geophys., 32, 621–642, https://doi.org/10.1007/s10712-011-9142-2, 2011.

Swart, N. C., Cole, J. N. S., Kharin, V. V., Lazare, M., Scinocca, J. F., Gillett, N. P., Anstey, J., Arora, V., Christian, J. R., Hanna, S., Jiao, Y., Lee, W. G., Majaess, F., Saenko, O. A., Seiler, C., Seinen, C., Shao, A., Sigmond, M., Solheim, L., von Salzen, K., Yang, D., and Winter, B.: The Canadian Earth System Model version 5 (CanESM5.0.3), Geosci. Model Dev., 12, 4823–4873, https://doi.org/10.5194/gmd-12-4823-2019, 2019.

Tatebe, H., Ogura, T., Nitta, T., Komuro, Y., Ogochi, K., Takemura, T., Sudo, K., Sekiguchi, M., Abe, M., Saito, F., Chikira, M., Watanabe, S., Mori, M., Hirota, N., Kawatani, Y., Mochizuki, T., Yoshimura, K., Takata, K., O'ishi, R., Yamazaki, D., Suzuki, T., Kurogi, M., Kataoka, T., Watanabe, M., and Kimoto, M.: Description and basic evaluation of simulated mean state, internal variability, and climate sensitivity in MIROC6, Geosci. Model Dev., 12, 2727–2765, https://doi.org/10.5194/gmd-12-2727-2019, 2019.

Todd, A., Zanna, L., Couldrey, M., Gregory, J., Wu, Q., Church, J. A., Farneti, R., Navarro-Labastida, R., Lyu, K., Saenko, O., Yang, D. and Zhang, X.: Ocean-only FAFMIP: Understanding regional patterns of ocean heat content and dynamic sea level change, J. Adv. Model. Earth Sy., 12, e2019MS002027, https://doi.org/10.1029/2019MS002027, 2020.

https://doi.org/10.5194/egusphere-2022-610
Preprint. Discussion started: 28 July 2022

Weijer, W., Cheng, W., Garuba, O. A., Hu, A. and Nadiga, B. T.: CMIP6 models predict significant 21st century decline of the Atlantic Meridional Overturning Circulation, Geophys. Res. Lett., 47, e2019GL086075, https://doi.org/10.1029/2019GL086075, 2020.

Wang, Y., Yu, Z., Lin, P., Liu, H., Jin, J., Li, L., Tang, Y., Dong, L., Chen, K., Li, Y., Yang, Q., Ding, M., Meng, Y., Zhao, B., Wei, J., Ma, J., and Sun, Z.: FGOALS-g3 model datasets for CMIP6 flux-anomaly-forced model intercomparison project, Adv. Atmos. Sci., 37, 1093-1101, https://doi.org/10.1007/s00376-020-2045-8, 2020.

Xie, P. and Vallis, G. K.: The passive and active nature of ocean heat uptake in idealized climate change experiments, Clim. Dynam., 38, 667-684, doi:10.1007/s00382-011-1063-8, 2012.

Yang, H., Wang, K., Dai, H, Wang, Y and Li, Q.: Wind effect on the Atlantic meridional overturning circulation via sea ice and vertical diffusion, Clim. Dynam., 46, 3387–3403, https://doi.org/10.1007/s00382-015-2774-z, 2016.

Yin J.: Century to multi‐century sea level rise projections from CMIP5 models, Geophys. Res. Lett., 46, 3387–3403, https://doi.org/10.1007/s00382-015-2774-z, 2012.

Yin J., Griffies S. M., and Stouffer R. J.: Spatial variability of sea level rise in twenty-first century projections, J. Climate, 23, 4585-4607, https://doi.org/10.1175/2010JCLI3533.1, 2010.

https://doi.org/10.5194/egusphere-2022-610
Preprint. Discussion started: 28 July 2022

Yukimoto, S., Kawai, H., Koshiro, T., Oshima, N., Yoshida, K., Urakawa, S., Tsujino, H., Deushi, M., Tanaka, T., Hosaka, M., Yabu, S., Yoshimura, H., Shindo, E., Mizuta, R., Obata, A., Adachi, Y. and Ishii, M.: The Meteorological Research Institute Earth System Model version 2.0, MRI-ESM2. 0: Description and basic evaluation of the physical component, J. Meteorol. Soc. Japan. Ser. II, https://doi.org/10.2151/jmsj.2019-051, 2019.

https://doi.org/10.5194/egusphere-2022-610
Preprint. Discussion started: 28 July 2022

Tables

Models	Ocean horizontal resolution	References
ACCESS-CM2	MOM 1→1/3° tripolar z	Kiss et al., 2020
CanESM5	ORCA1→1/3° tripolar 46z	Swart et al., 2019
CAS- ESM2	LICOM2 1→1/2° 30z	Jin et al., 2021
FGOALS-g3	LICOM3 1→1/3° 30z	Li et al., 2020
GFDL-ESM2M	MOM5 1→1/3° 50z	Dunne et al., 2012
MPI-ESM1.2-HR	MPIOM1.65 0.4° tripolar 40z	Mauristsen et al., 2019
MRI-ESM2.0	MRI.COMv4 1° x 0.5° tripolar 61z	Yukimota et al., 2019
MIROC6	COCO4.9 1° tripolar 63z	Tatebe et al., 2019

Table 1 Key features of the main AOGCMs studied.

https://doi.org/10.5194/egusphere-2022-610
Preprint. Discussion started: 28 July 2022

	Experiments \ models	ACCESS	CanESM5	CAS-ESM2	FOGALS-g3	GFDL-ESM2M	MPI-ESM1-2-HR	MRI-ESM2-0	MIROC6
T	heat	○	○	○	○	○	○	○	○
	NA50	○	○	○	○	○	○	○	○
	NA0	○	○	○	○	○	×	○	○
AMOC	heat	○	○	○	○	×	○	○	○
	NA50	○	○	○	○	×	○	○	○
	NA0	○	○	○	○	×	×	○	×
DSL	heat	○	○	○	○	○	○	○	○
	NA50	○	○	○	○	○	○	○	×
	NA0	○	○	○	○	○	×	○	×
T_a'	heat	×	×	○	○	○	○	○	×
	NA50	×	×	○	×	○	○	○	×
	NA0	×	×	○	×	○	×	○	×
T_r'	heat	×	×	○	×	○	○	○	×
	NA50	×	×	○	×	○	○	○	×
	NA0	×	×	○	×	○	×	○	×
Salinity	heat	○	○	○	○	○	○	○	○
	NA50	○	○	○	○	○	○	○	○
	NA0	○	○	○	○	○	×	○	○
Q_r'	heat	○	○	○	○	○	○	○	○
	NA50	○	○	○	○	○	○	○	○
	NA0	○	○	○	○	○	×	○	×

Table 2 Available output data: Available: ○; not available: ×.

https://doi.org/10.5194/egusphere-2022-610
Preprint. Discussion started: 28 July 2022

Figures

Figure 1 Annual time series of the weakening of the maximum of the Atlantic meridional overturning stream function (unit: Sv) of different AOGCMs, all showing the difference between faf-heat, faf-heat-NA50pct and faf-heat-NA0pct and the corresponding year of the control. The black solid line indicates the ensemble-mean results, and different colors indicate different results for the AOGCMs.

Figure 2 The ensemble-mean redistributed heat flux Q_r' (unit: W m^{-2}) due to the circulation change for faf-heat (a), faf-heat-NA50pct (b) and faf-heat-NA0pct (c). (d) and (e) indicate the difference between the faf-heat-NA50pct and faf-heat and the difference between the faf-heat-NA0pct and faf-heat.

Figure 3 Top row shows the annual time series of the volume-mean ocean temperature change T' (Unit: °C); (d), (e) and (f) are the same as (a), (b) and (c), but for the added temperature changes, $T_a{}'$ (Unit: °C); all show the differences between faf-heat (left), faf-heat-NA50pct (center) and faf-heat-NA0pct (right) and corresponding years for the control. The black solid line indicates the ensemble-mean T', and the black dashed line indicates the ensemble-mean $T_a{}'$. Different colors indicate the results for different AOGCMs.

Figure 4 Vertical profiles of ensemble-mean zonal-mean temperature change, T'(Unit: °C) and added temperature changes $T_a{}'$(Unit: °C) in the time-mean for years 61–70 for faf-heat, faf-heat-NA50pct and faf-heat-NA0pct relative to the control for different basins: the Southern Ocean (left), Pacific–Indian Ocean (middle), and

https://doi.org/10.5194/egusphere-2022-610
Preprint. Discussion started: 28 July 2022

Arctic–Atlantic Ocean (right). Black, red and blue lines denoting experiments of faf-heat, faf-heat-NA50pct and faf-heat-NA0pct, respectively. Lines with lighter colors indicate temperature changes of different AOGCMs.

Figure 5 Spatial patterns of the ensemble-mean total ocean heat uptake (OHU) (top), added portions (OHUa) (middle) and redistributed portions (OHUr) (bottom) (unit: GJ/m^2, vertical integral of the change in the tracer multiplied by the volumetric heat capacity), averaged for the time-mean of years 61–70 for faf-heat (left), faf-heat-NA50pct (center) and faf-heat-NA0pct (right) relative to the control.

Figure 6 Spatial patterns of the ensemble standard deviation of total ocean heat uptake (OHU) (top), added portions (OHUa) (middle) and redistributed portions (OHUr) (bottom) (unit: GJ/m^2), averaged for the time-mean for years 61–70 for faf-heat (left), faf-heat-NA50pct (center) and faf-heat-NA0pct (right) relative to the control.

Figure 7 Spatial patterns of the ensemble-mean change in the dynamic sea level (DSL) (first row), thermosteric sea level (TSSL) (second row) and halosteric sea level (HSSL) (bottom row) (unit: m), averaged for the time-mean of years 61–70 for faf-heat (left), faf-heat-NA50pct (center) and faf-heat-NA0pct (right) relative to the control in the experiments.

Figure 8 Spatial patterns of the ensemble standard deviation of the dynamic sea level (DSL) (first row), thermosteric sea level (TSSL) (second row) and halosteric sea level (HSSL) (bottom row) (unit: m), averaged for the time-mean of years 61–70 for faf-heat (left), faf-heat-NA50pct (center) and faf-heat-NA0pct (right) relative to the control in the experiments.

https://doi.org/10.5194/egusphere-2022-610
Preprint. Discussion started: 28 July 2022

Figures

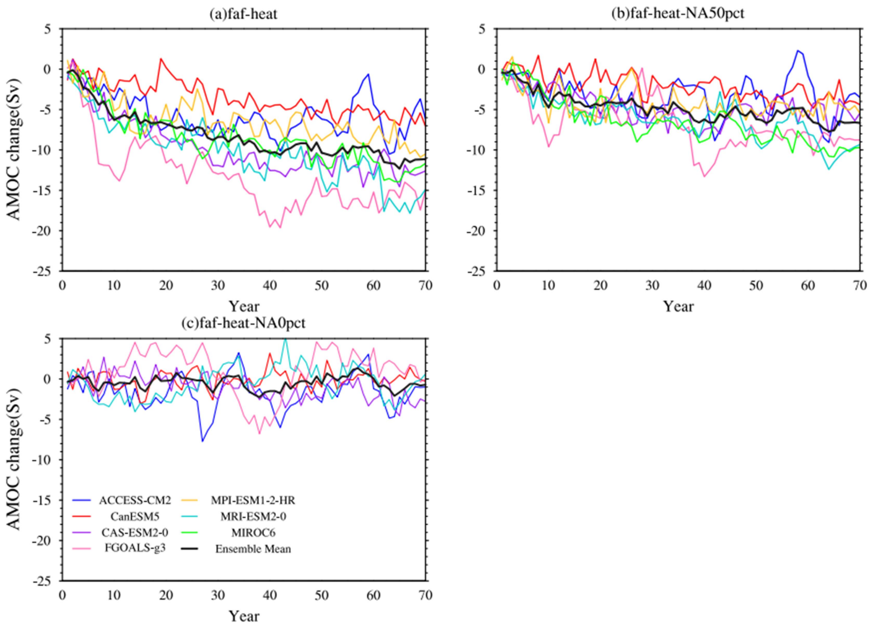

Figure 1 Annual time series of the weakening of the maximum of the Atlantic meridional overturning stream function (unit: Sv) of the different AOGCMs, all showing the difference between faf-heat, faf-heat-NA50pct and faf-heat-NA0pct and corresponding year of the control. The black solid line indicates the ensemble-mean results, and different colors indicate different results for the AOGCMs.

https://doi.org/10.5194/egusphere-2022-610
Preprint. Discussion started: 28 July 2022

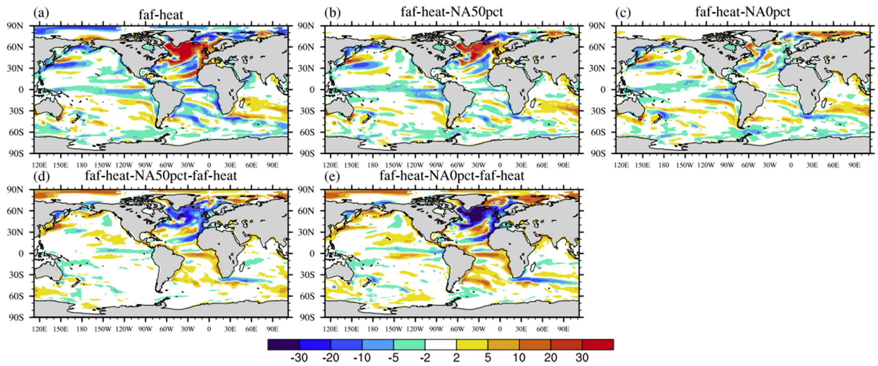

Figure 2 The ensemble-mean redistributed heat flux Q_r' (unit: W m^{-2}) due to the circulation change for faf-heat (a), faf-heat-NA50pct (b) and faf-heat-NA0pct (c). (d) and (e) indicate the difference between the faf-heat-NA50pct and faf-heat and the difference between the faf-heat-NA0pct and faf-heat.

https://doi.org/10.5194/egusphere-2022-610
Preprint. Discussion started: 28 July 2022

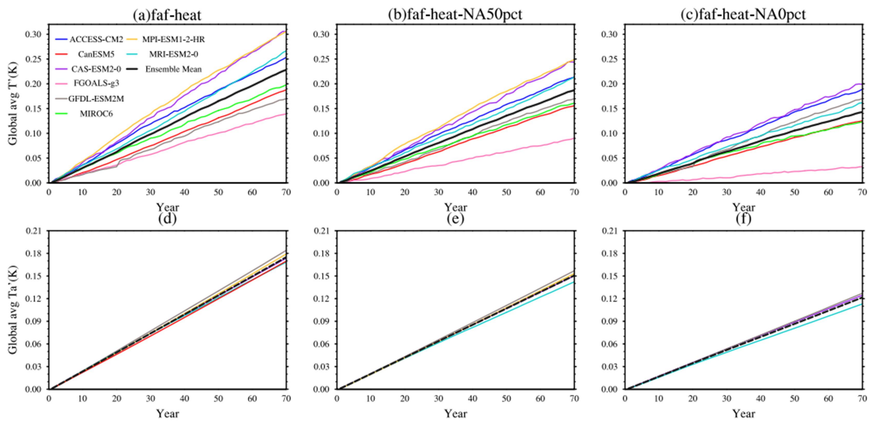

Figure 3 Top row shows the annual time series of the volume-mean ocean temperature change, T'(Unit: °C). (d), (e) and (f) are the same as (a), (b) and (c), but for the added temperature changes, $T_a{}'$(bottom row) (Unit: °C), all showing the differences between faf-heat (left), faf-heat-NA50pct (center) and faf-heat-NA0pct (right) and corresponding years of the control. The black solid line indicates the ensemble-mean T', and the black dashed line indicates the ensemble-mean $T_a{}'$. Different colors indicate the results of different AOGCMs.

https://doi.org/10.5194/egusphere-2022-610
Preprint. Discussion started: 28 July 2022

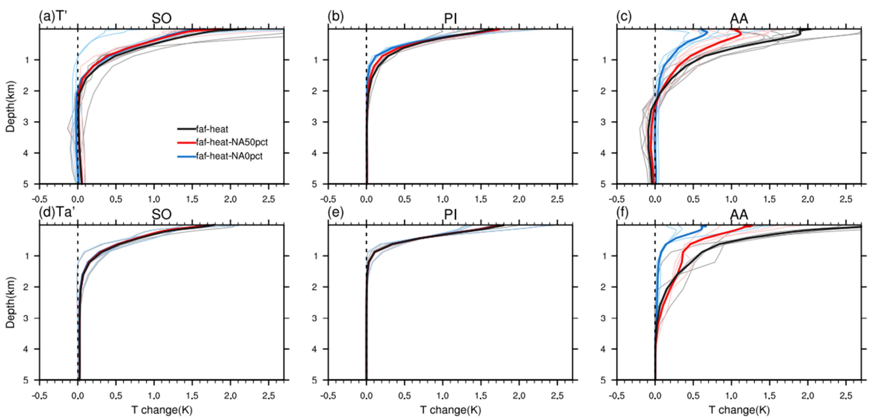

Figure 4 Vertical profiles of ensemble-mean zonal-mean temperature change T' (top row) (Unit: ℃) and added temperature changes, $T_a{}'$ (bottom row) (Unit: ℃) in the time-mean of years 61–70 for faf-heat, faf-heat-NA50pct and faf-heat-NA0pct relative to the control for different basins: the Southern Ocean (left), Pacific–Indian Ocean (middle), and Arctic–Atlantic Ocean (right). Black, red and blue lines denote the faf-heat, faf-heat-NA50pct and faf-heat-NA0pct experiments, respectively. Lines with lighter colors indicate temperature changes for different AOGCMs.

https://doi.org/10.5194/egusphere-2022-610
Preprint. Discussion started: 28 July 2022

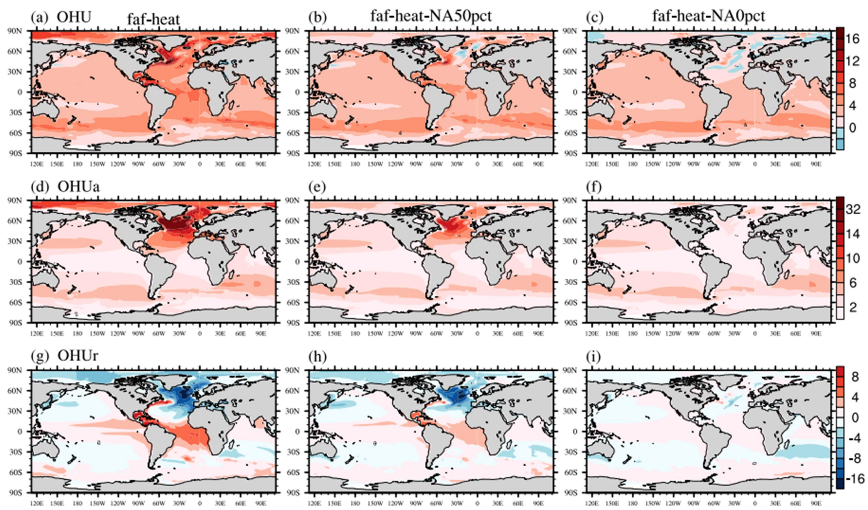

Figure 5 Spatial patterns of the ensemble-mean total ocean heat uptake (OHU) (top), added portions (OHUa) (middle) and redistributed portions (OHUr) (bottom) (unit: GJ/m^2, vertical integral of the change in the tracer multiplied by the volumetric heat capacity), averaged for the time-mean of years 61–70 for faf-heat (left), faf-heat-NA50pct (center) and faf-heat-NA0pct (right) relative to the control.

https://doi.org/10.5194/egusphere-2022-610
Preprint. Discussion started: 28 July 2022

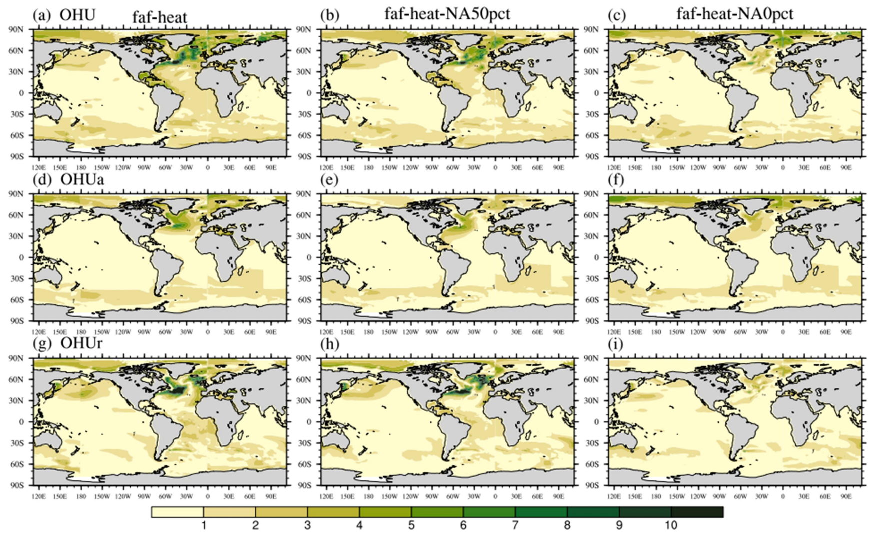

Figure 6 Spatial patterns of the ensemble standard deviation of total ocean heat uptake (OHU) (top), added portions (OHUa) (middle) and redistributed portions (OHUr) (bottom) (unit: GJ/m^2), averaged for the time-mean of years 61–70 for faf-heat (left), faf-heat-NA50pct (center) and faf-heat-NA0pct (right) relative to the control.

https://doi.org/10.5194/egusphere-2022-610
Preprint. Discussion started: 28 July 2022

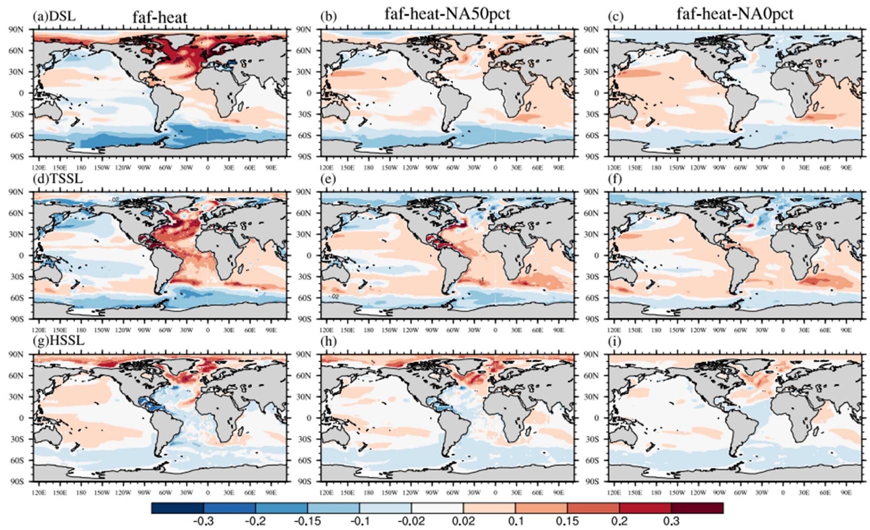

Figure 7 Spatial patterns of the ensemble-mean change in the dynamic sea level (DSL) (first row), thermosteric sea level (TSSL) (second row) and halosteric sea level (HSSL) (bottom row) (unit: m), averaged for the time-mean of years 61–70 for faf-heat (left), faf-heat-NA50pct (center) and faf-heat-NA0pct (right) relative to the control in the experiments.

https://doi.org/10.5194/egusphere-2022-610
Preprint. Discussion started: 28 July 2022

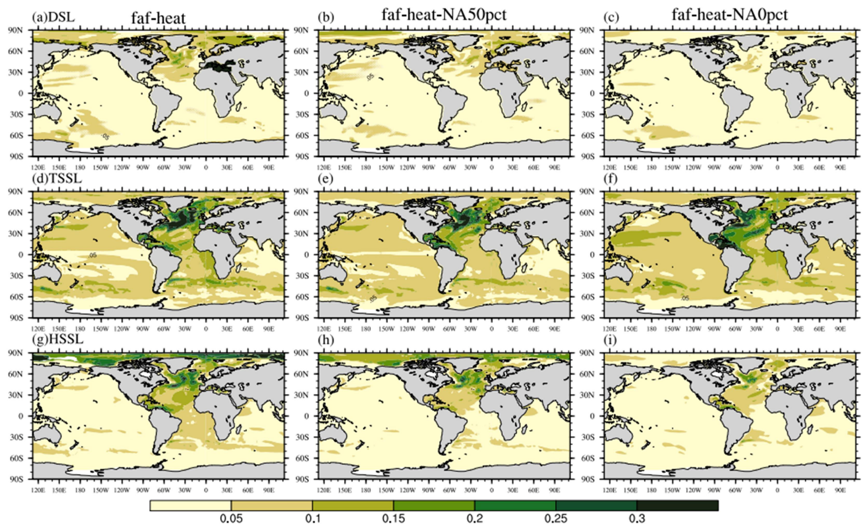

Figure 8 Spatial patterns of the ensemble standard deviation of the dynamic sea level (DSL) (first row), thermosteric sea level (TSSL) (second row) and halosteric sea level (HSSL) (bottom row) (unit: m), averaged for the time-mean of years 61–70 for faf-heat (left), faf-heat-NA50pct (center) and faf-heat-NA0pct (right) relative to the control in the experiments.

Data avavilability

All data acquired or used in this analysis are available from CMIP6 website (CMIP6; https://esgf-node.llnl.gov/projects/cmip6/), obtained between 20 June 2021 and 30 June 2021.

Auther Contribution

YW performed data analysis and prepared the paper. JJ and ZG provided advice on the analysis and the paper.

https://doi.org/10.5194/egusphere-2022-610
Preprint. Discussion started: 28 July 2022

Competing interests

The contact author has declared that neither they nor their co-authors has any competing interests.